Journal of Applied Electrochemistry (2005) 35:625–631
DOI 10.1007/s10800-005-2573-z
© Springer 2005

Electrochemical oxidation of phenolic compounds using a flow-through electrolyser with porous solid electrodes

R. MENINI[1,*], Y.M. HENUSET[2] and J. FOURNIER[3]
[1]*National Research Council Canada, Industrial Materials Institute, 75, de Mortagne Blvd., Boucherville (QC), J4B 6Y4, Canada*
[2]*Global-Ionix, 25 AA De Lauzon, Boucherville (QC), J4B 1E7, Canada*
[3]*Centre d'études des procédés chimiques du Québec (CÉPROCQ), 6220Sherbrooke E., Montréal, (QC), H1N 1C1, Canada*
*(*author for correspondence, fax: +1-450-641-5105; e-mail: richard.menini@imi.cnrc-nrc.gc.ca)*

Received 20 September 2003; accepted in revised form 09 February 2005

Key words: cresol, electrochemical oxidation, flow-through, foam, oxidation, phenol, wastewater

Abstract

Organic compounds such as phenol and cresols may be found in industrial wastewater along with other organics and are difficult to be economically removed down to concentrations below environmentally permissible limits. By circulating a wastewater through an electrolytic reactor with a stack of porous solid anodes and cathodes, it has been demonstrated that it is feasible to electrochemically oxidize phenolic compounds in the presence of other organic molecules. A porous solid DSA®-type titanium anode coated with several mixed oxide layers was used as the active material. At low applied current densities, phenol and cresol concentrations were reduced from 5000 ppb to below 20 ppb. The influence of the flow rate and electrodes number was also studied and it was demonstrated that the current density was the main factor to be considered. This work confirms the hypotheses of other authors on the reaction mechanisms involved during the electrochemical oxidation of cresol and phenol.

1. Introduction

Environmental regulations of the Province of Quebec forbid the release of effluent in water if the phenol, *o*-cresol and *p*-cresol concentrations are above 20, 38 and 6.2 ppb respectively [1] at $6 < pH < 9.5$ [2]. Some industrial effluents may contain more than 5000 ppb of phenolic compounds that are found together with other organic species. Several non-electrolytic processes for phenol decontamination already have been explored: enzyme catalysed oxidation [3], photocatalysis [4, 5], bacteria seeding (anaerobic process) [6], chemical oxidation (H_2O_2 or O_3) [7] as well as the use of polymeric adsorbents [8]. All these methods have some advantages and drawbacks such as material cost or equipment size limitation when large volumes of water need to be treated. Electrochemical oxidation methods used alone or coupled with other treatment techniques can be more economically viable as well as more efficient for the treatment of phenols [9–13].

This paper describes a promising new electrochemical method to destroy phenolic compounds [14] by treating wastewater with only two pre-treatment steps: pH adjustment and filtration. The contaminated solution was circulated into a flow-through electrolytic reactor fitted with porous DSA®-type anodes to oxidize organic compounds such as phenol and cresols. The use of porous DSA®-type anodes led to the decontamination of wastewater containing the above-mentioned pollutants, despite the fact that these substances were found among many other organic compounds. Both high mass transport, self promoted by the porous structure of the electrodes, and high electrode surface area were expected to increase oxidation rates. Additionally, the effects of current density, flow rate, number of electrodes and long-term electrolysis upon oxidation efficiency were studied. Finally, this work confirms the hypotheses of other authors on the reaction mechanisms involved during the electrochemical oxidation of cresol and phenol.

2. Experimental

2.1. *Solution analysis and pre-treatment*

A Horiba chemical analyser evaluated the total organic content (TOC) of the raw wastewater. As far as the pre-treatment steps were concerned, the pH was adjusted using a 1 M NaOH solution, while, to remove solid particles, the wastewater was decanted and filtered using a ''42 Whatman'' filter paper. The solid obtained after filtration was analysed by X-ray energy dispersion

spectrometry using a JEOL 1400 SEM. Phenol and *o*-, *m*- and *p*-cresol concentrations were determined using a GC/MS SIM apparatus. The pH of the solution was evaluated using an Orion pH-meter Model 710A whilst the conductivity was measured before and after the adjustment of the solution pH using a Radiometer Copenhagen CDM 83 system.

2.2. *Electrode materials*

The anode substrate, produced by *AstroMet*, consisted of a spongy titanium structure having the following characteristics: 20-ppi (pores per linear inch), 3 cm in diameter, 0.5 cm thick and a 14 cm^2/cm^3 real surface area that represented a total available surface area of 35.45 cm^2 for each electrode. All the current densities were calculated according to this surface area. Prior to the coating steps, titanium foams were solvent degreased followed by etching in boiling concentrated hydrochloric acid during 3 min; subsequently, they were thoroughly rinsed and coated with a DSA®-type material using the thermal decomposition technique [15]. The porous titanium substrates were covered with four layers of antimony-doped tin oxide over two layers of iridium dioxide according to the method described in [16]. Foams were immersed in a 4% (w/w) $IrCl_4$ solution of ethanol followed by two heat treatments first at 80 °C for 10 min in an air-circulating oven and then at 500 °C for 30 min in a furnace; the furnace was then shut down and allowed to cool slowly prior to electrode removal. These steps were repeated one more time to produce two IrO_2 layers. Electrodes were then immersed in an isopropanol solution (20% $SnCl_4 \cdot 5H_2O$ and 0.2% $SbCl_3$) and heat-treated according the above-mentioned two heating steps. To ensure that the electrode material in contact with the wastewater was tin dioxide, four layers of antimony-doped tin dioxide were deposited [15]. The spongy nickel cathode material, made by *AstroMet*, had the same dimensions and porous structure as the above-mentioned titanium anode substrates.

2.3. *Electrochemical reactor*

The flow-through single unit reactor consisted of a 4-cm diameter Lucite tube with two inlet and outlet plugs fitted at each end where tubing was mounted, see Figure 1. A peristaltic pump providing constant flow rates of 1.7 or 8.2 l min^{-1} was used in a closed-loop circulation fashion while the wastewater was kept in a 3-litre beaker. The outlet plug had an internal funnel shape to avoid liquid flow-back. Each 3-D electrode (3 anodes and 4 cathodes) was mounted between two Lucite disk holders and placed in a slot perpendicular to the liquid flow. The electrical connections consisted of spot-welded titanium wires for the anodes and nickel wires for the cathodes and were fitted across the tube through small holes sealed with epoxy glue. In order to double the number of electrodes, two single unit reactors were linked together in series.

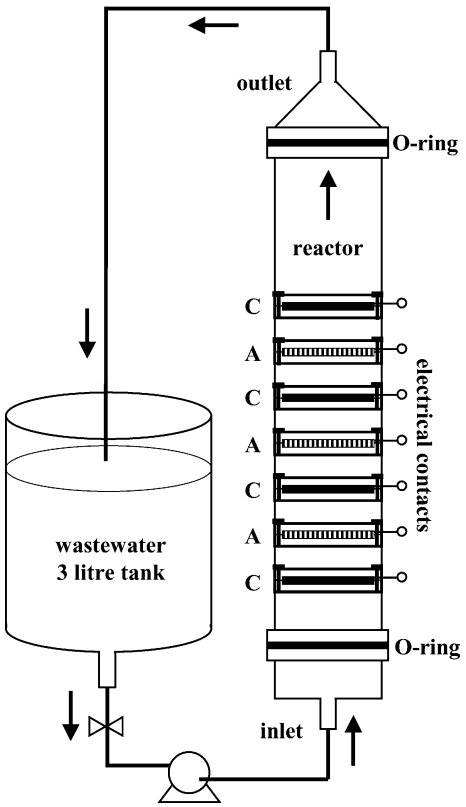

Fig. 1. Schematic representation of a single electrochemical reactor. **C** is cathode and **A** is anode.

3. Results and discussion

3.1. *Solution analysis and pre-treatment*

An industrial wastewater having a TOC level of about 5000 ppm constituted the raw solution to be studied. The total concentration level of *o*-, *m*-, *p*-cresol and phenol was found to be around 3500 ppb while the pH was equal to 5.5 ± 0.5. Since this pH value was not within the acceptable environmental limits [2], it was adjusted to 8.0. As a consequence of this treatment, precipitation of greenish brown particles occurred. The solid formed, representing roughly 0.4% w/v, was filtered and analysed by X-ray energy dispersion spectrometry. The filtrate was mainly composed of 80–85% of inorganic species such as Fe_2O_3, SiO_2 and traces of aluminium and manganese oxides. The filtration step was necessary in order to avoid electrode plugging during electrolysis.

3.2. *Anode characterisation*

The main objective of the present study was to oxidize phenol and cresol compounds using a flow-through system that can lead to high self-turbulent hydrodynamic conditions and provided a large active surface

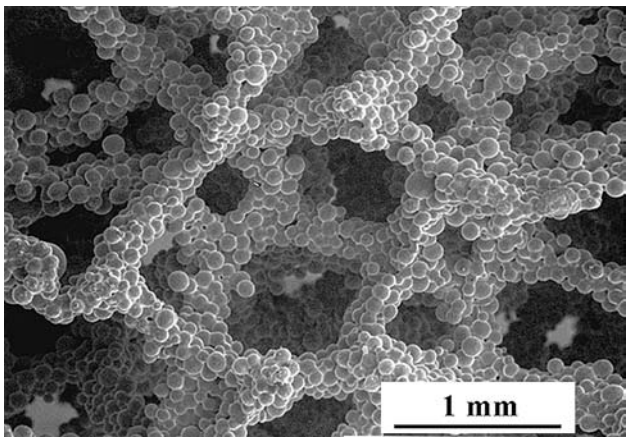

Fig. 2. SEM micrograph of a 20-ppi spongy titanium substrate.

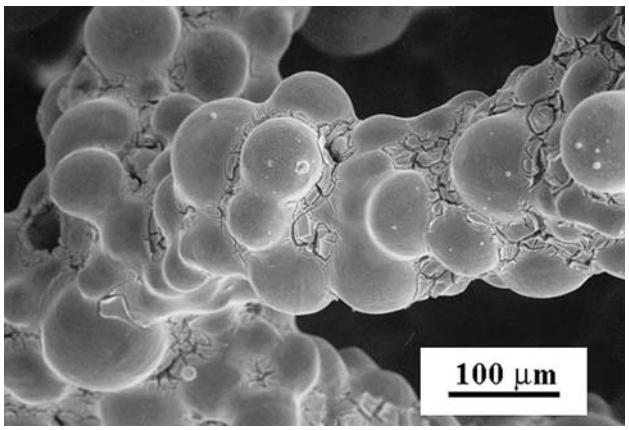

Fig. 3. SEM micrograph of the 20-ppi spongy Ti material after deposition of two IrO_2 layers.

area for the electrochemical reactions [17]. In view of the fact that anode material for electrochemical oxidation of organic species was thoroughly investigated in the literature, its choice was oriented towards one of the best materials for organic electrochemical oxidation: Ti/IrO_2/SnO_2/Sb_2O_5 [18]. Therefore, the efforts were focused on the choice of a new type of 3-D Ti anode substrate for these oxides as well as on the deposition processes of iridium, tin and antimony oxides on such a porous solid structure.

Figure 2 shows the 20-ppi spongy type titanium material that was used as the anode substrate and was approximately 90% porous, according to the manufacturer's material data sheet. This material was selected because of its ability to let a liquid pass through without a high-pressure drop and its solid structure that provided a better conductive medium compared to a fluidised bed type of electrode [9, 19].

Since the thickness of the electrodes was 5 mm, a 2.5 mm thickness of active material was available on each side of the anode. Figure 3 shows the 20-ppi spongy material after deposition of the IrO_2 underlayers. The coating tended to accumulate mainly at the interstices between the titanium particles where crack formation occurred. Figure 4 shows the electrode network after the final coating application and it can be observed that the pores were big enough so that no clogging during the electrolysis can take place. The resulting deposit that underwent several temperature cycles revealed the usual stress-cracking pattern associated with the thermal decomposition technique, as shown in Figure 5.

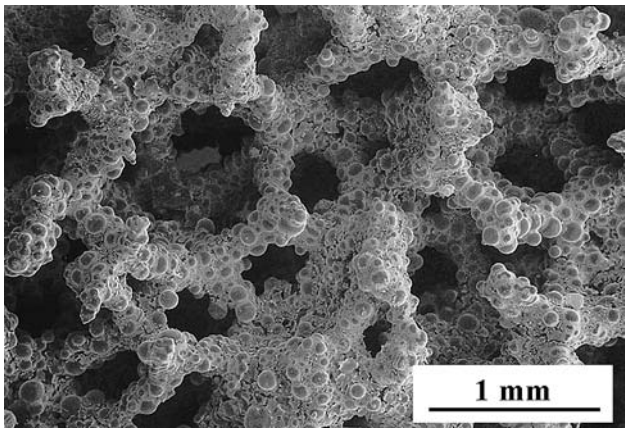

Fig. 4. SEM micrograph of the DSA®-type of anode having the composition: Ti/IrO_2/SnO_2/Sb_2O_5.

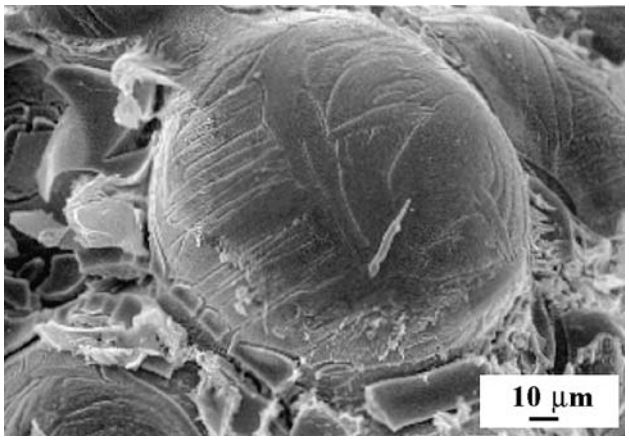

Fig. 5. High magnification SEM micrograph of the DSA®-type of anode (Ti/IrO_2/SnO_2/Sb_2O_5).

3.3. *Efficiency as a function of current density*

Figures 6 and 7 display the plots of phenol and cresol concentrations vs. charge at 5.6 and 2.8 mA cm^{-2} current densities, respectively. Comparison between these two figures clearly shows that the high current density gave a lower oxidation performance since, at 5.6 mA cm^{-2} and after 26 kC, only the *o*-cresol was removed while the *p*-cresol and the phenol concentrations were well above the 20 ppb mark, see Figure 6. On the other hand, at 2.8 mA cm^{-2}, no *o*- and *m*-cresol were detected, while the concentration of phenol was under the 20 ppb value and the *p*-cresol was just above this value, see Figure 7.

To assess the real influence of each parameter on reaction efficiency, phenol, *m*-cresol and *p*-cresol slope

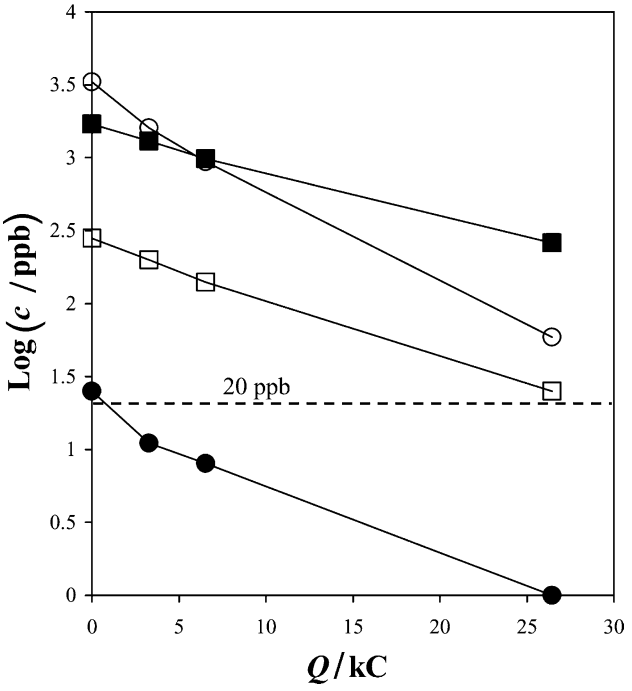

Fig. 6. Phenol and cresols concentrations vs. charge. Electrolysis conditions: one unit reactor type, $j = 5.6$ mA cm^{-2} and $v = 8.2$ l min^{-1}. (○): *p*-cresol, (■): phenol, (□): *m*-cresol and (●): *o*-cresol.

calculations for the curves, Log [*c*] = f (*Q*), were performed between 0 and 20 kC. All the results are displayed in Table 1 where the slopes (*S*) are directly associated to reaction efficiencies. In this table, the average efficiency ($\bar{S}$) corresponds to the average phenol, *p*-cresol and *m*-cresol efficiencies. The slope of the *o*-cresol was not analysed since this molecule was found in low concentration and because few points were available for accurate slope measurements. Finally, average efficiency ratios (R_E) were evaluated to assess the influence of the experimental conditions upon each other. As expected from the observation of Figures 6 and 7, one can see that R_E was almost doubled (1.86) when the current was set at 2.8 mA cm^{-2} compared to 5.6 mA cm^{-2}.

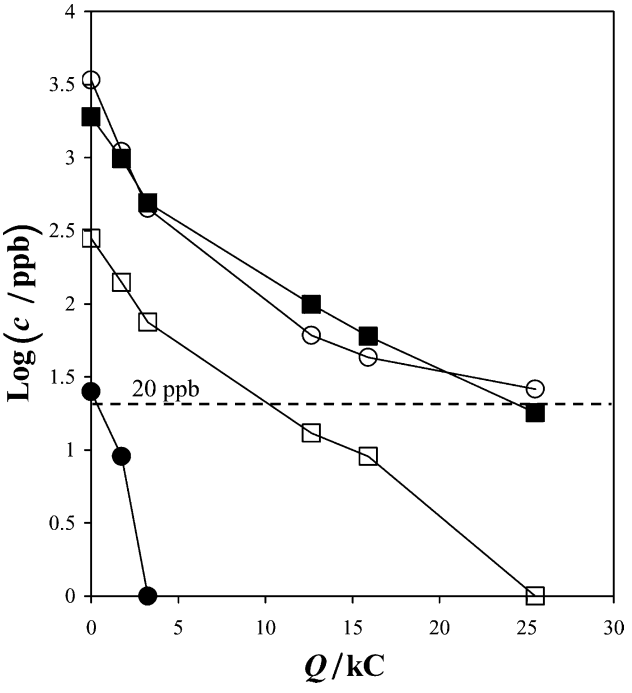

Fig. 7. Phenol and cresols concentrations vs. charge. Electrolysis conditions: one reactor unit type, $j = 2.8$ mA cm^{-2} and $v = 8.2$ l min^{-1}. (○): *p*-cresol, (■): phenol, (□): *m*-cresol and (●): *o*-cresol.

The effect of current density on reaction efficiency was reported by Comninellis and Nerini [18] for phenol oxidation in the presence of NaCl. The explanation for such a behaviour can be found in another work by Comninellis [20] where it is described that the electrochemical oxidation mechanism of organics involve the formation of adsorbed hydroxyl radicals $MO_x(^{\bullet}OH)$ according to the following equation:

$$MO_x + H_2O \rightarrow MO_x(^{\bullet}OH) + H^+ + e^- \quad (1)$$

Hydroxyl radical formation was found to be very important on surface oxides particularly when M was Sn [18]. Hydroxyl radicals can then react with an organic molecule (R) and possibly lead to its entire combustion:

$$R + MO_x(^{\bullet}OH)_z \rightarrow CO_2 + ZH^+ + Ze^- + MO_x \quad (2)$$

Meanwhile, hydroxyl radicals may also react in another fashion to produce oxygen according to the ((3) and (4)) and/or (5) mechanisms:

$$MO_x(^{\bullet}OH) \rightarrow H^+ + e^- + MO_{x+1} \quad (3)$$

$$MO_{x+1} \rightarrow 1/2O_2 + MO_x \quad (4)$$

$$MO_x(^{\bullet}OH) \rightarrow 1/2O_2 + H^+ + e^- + MO_x \quad (5)$$

In fact, low current densities allowed the hydroxyl radicals to participate in the organic combustion (2) while high current densities favoured the competitive oxygen evolution reaction ((3) and (4)) or (5). Leffrang et al. [21] also reported this influence where the current efficiency was lowered when the applied current density was increased for phenol and chlorophenol electrochemical oxidations. A similar behaviour also can be observed in electrocatalytic hydrogenation, where, in this case, the hydrogen evolution reaction competes with the organic compound hydrogenation [22, 23].

3.4. *Influence of flow rate and number of reactors*

In order to investigate the effects of reactor configuration and flow rate upon reaction efficiencies, electrolyses were performed with two reactor configurations (single and double modes) and at two different flow rates (1.7 and 8.2 l min^{-1}). All the results are presented in Figures 8–10 and in Table 1. To remain in the linear domain, slope evaluations were performed between 0 and 30 kC for the results displayed in Figure 8 and between 0 and 12 kC for those shown in Figures 9 and 10. Overall, the regression coefficients were all above 0.97 for each slope assessment.

Table 1. Reaction efficiencies for different electrolysis conditions

	Experimental conditions				
	A	*B*	*C*	*D*	*E*
j (mA cm^{-2})	5.6	5.6	5.6 and 2.8	2.8	5.6 and 2.8
ν (l min^{-1})	8.2	1.7	8.2	8.2	1.7
Number of reactors	1	1	2	1	2
	Efficiencies, S (10^3 ppb C^{-1})				
	S_A	S_B	S_C	S_D	S_E
Phenol	− 0.030	− 0.052	− 0.068	− 0.077	− 0.070
m-cresol	− 0.039	− 0.057	− 0.059	− 0.091	− 0.079
p-cresol	− 0.064	− 0.061	− 0.138	− 0.080	− 0.126
Average $\bar{S}$	− 0.045	− 0.056	− 0.088	− 0.083	− 0.092
	Efficiency ratio				
	$\bar{S}_D/\bar{S}_A$	$\bar{S}_B/\bar{S}_A$	$\bar{S}_E/\bar{S}_C$	$\bar{S}_C/\bar{S}_A$	$\bar{S}_C/\bar{S}_D$
R_E	1.86	1.26	1.04	1.98	1.07

The global efficiency of the phenolic compound oxidation was excellent for electrolyses *C* to *E* since a 20 ppb concentration of *p*-cresol was reached after 80 kC, approximately. The influence of the flow rate upon reaction efficiency that was difficult to observe in the figures can be more easily assessed using the slope values shown in Table 1. Comparing a slower flow rate (*B*) to a faster one (*A*), the R_E value was 1.26 for a one-unit reactor at 5.6 mA cm^{-2}. In fact, the residence time of the molecules to be destroyed increased with a decrease of the flow rate, thus leading to higher reaction efficiencies. On the other hand, using a two-unit reactor system configuration, and comparing the two flow rates (*E* and *C*), it can be seen that the low flow rate marginally influences the overall reaction efficiency (R_E = 1.04) indicating that the influence of the current density was crucial compared to the flow rate influence.

The importance of the current density over the total electrode surface available for the reaction was also demonstrated. When two reactors were coupled in series (one at 2.8 and the other at 5.6 mA cm^{-2}, configuration *C* in Table 1) the reaction efficiency was doubled (R_E = 1.98) compared to the single reactor mode at 5.6 mA cm^{-2} (*A*). Meanwhile, comparing the same double-reactor configuration (*C*) with one single reactor set at 2.8 mA cm^{-2} (*D*), showed that the reaction efficiency was marginally improved (R_E = 1.07) for the first case. Therefore, the current density must be optimised first before increasing the total available surface area for the reaction.

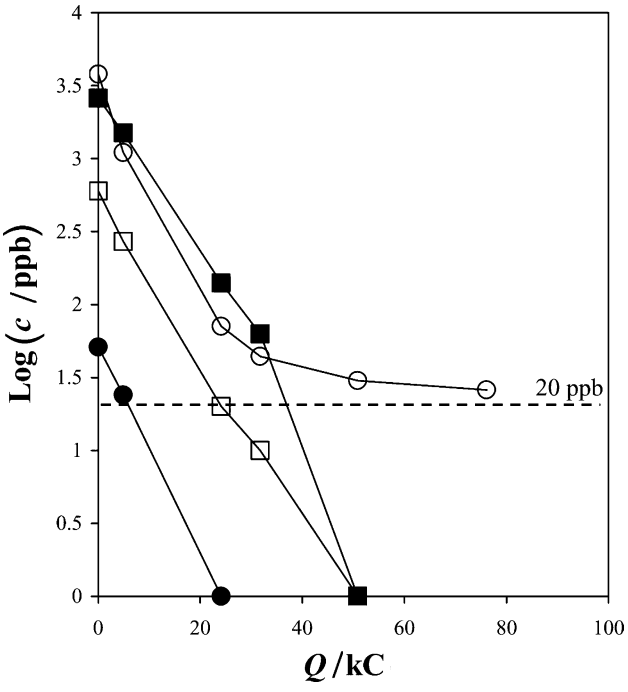

Fig. 8. Phenol and cresols concentrations vs. charge. Electrolysis conditions: one reactor unit type, j = 5.6 mA cm^{-2} and ν = 1.7 l min^{-1}. (○): *p*-cresol, (■): phenol, (□): *m*-cresol and (●): *o*-cresol.

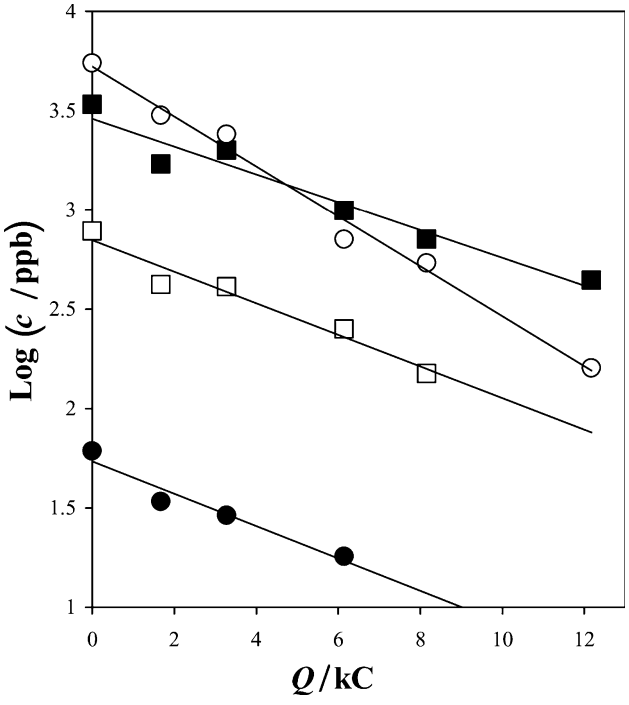

Fig. 9. Phenol and cresols concentrations vs. charge. Electrolysis conditions: two reactors in series, j = 2.8 and 5.6 mA cm^{-2}, ν = 8.2 l min^{-1}. (○): *p*-cresol, (■): phenol, (□): *m*-cresol and (●): *o*-cresol.

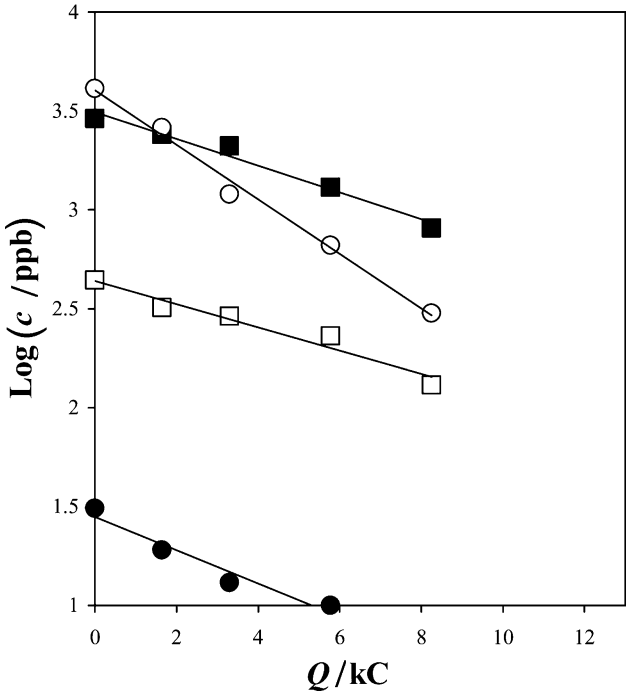

Fig. 10. Phenol and cresols concentrations vs. charge. Electrolysis conditions: two reactors in series, $j = 2.8$ and 5.6 mA cm^{-2}, $v = 1.7$ l min^{-1}. (○): *p*-cresol, (■): phenol, (□): *m*-cresol and (●): *o*-cresol.

3.5. *Reproducibility and reliability*

One set of anodes was used for as many as 20 electrolyses, which corresponded to more than 1000 hours of use. Following electrochemical oxidations, both anodes and cathodes were covered by a film that was probably organic; in fact, the anodes became orange–brown while the cathodes became black. This colour change was also observed by Comninellis and Pulgarin [24] on anodes made of platinum and, according to these authors, was due to the formation of a conductive polymer film. Further studies must be performed to investigate the film formation on the surface of the oxides. However, it is important to point out that the potential recorded during different electrochemical oxidation experiments, did not vary significantly from one experiment to another. Most importantly, and after 1000 h of electrolysis, reaction efficiencies were not altered and no clogging of the electrode pores was observed.

3.6. *Reaction mechanisms*

The *p*-cresol oxidation showed a different behaviour compared to the phenol and the *m*- and *o*-cresol. Firstly, total oxidation was never achieved and a plateau was reached near 20 ppb at high Q values, see Figures 7 and 8. Secondly, at low Q values, the *p*-cresol oxidation reaction rate exhibited better efficiency (steeper slope) compared to the three other reactions, see Figures 9 and 10. In fact, phenol and *m*-cresol showed a very similar rate of destruction while the *p*-cresol disappeared twice as rapidly, see Table 1, S_C and S_E. To investigate this behaviour, the proposed mechanisms found in the literature for the phenol and *p*-cresol oxidations [4, 5] were examined. It must be pointed out that these two studies were not carried out electrochemically: adsorbed OH radicals were obtained by aqueous H_2O_2 photolysis on polyoxometallates (POM) [4] or by aerobic irradiation in aqueous suspensions of TiO_2 [5]. According to Mylonas et al. [4], the main path to oxidize the *p*-cresol consists in the methyl group removal through a mechanism involving alcohol, aldehyde and acid molecules. In fact, according to these authors, the methyl group in the para position favours its own removal compared to the meta and ortho positions. Mylonas et al. [4] confirmed experimentally that the hydroxyl radical attack for the *p*-cresol degradation exhibited a better efficiency than that of the phenol oxidation; see Figs 1a and 2a of [4]. Additionally, Preis et al. [5] observed the same activation due the methyl group present in the para position. In the present work, the different intermediate compounds were not analysed due to the high TOC value of the raw solution. However, as far as *p*-cresol oxidation was concerned, similar results in terms of reactivity were obtained using the three different oxidation techniques described in other research [4, 5] and in the present work. Therefore, indirect oxidation was probably the mechanism encountered on the Ti/IrO_2/SnO_2/Sb_2O_5 anodes for destruction of phenolic compounds. Further studies using cyclic voltammetry of 15 ppm of phenol in a 1 M Na_2SO_4 aqueous solution confirmed the latter statement since no oxidation wave was detected apart from the one due to the oxygen evolution reaction.

Concerning the plateau reached for the *p*-cresol oxidation, see Figures 7 and 8, carbon dioxide production, see Equation 2, at the anode can lead to the formation of bicarbonate and carbonate according to the following reactions [25]:

For pH < 8:

$$CO_2 + H_2O \leftrightarrow H_2CO_3 \quad \text{(slow)} \tag{6}$$

$$H_2CO_3 + OH^- \leftrightarrow HCO_3^- + H_2O \quad \text{(fast)} \tag{7}$$

For pH > 10:

$$CO_2 + OH^- \leftrightarrow HCO_3^- \quad \text{(slow)} \tag{9}$$

$$HCO_3^- + OH^- \leftrightarrow CO_3^{2-} + H_2O \quad \text{(fast)} \tag{9}$$

Since bicarbonate and carbonate ions are well known radical scavengers [25], they can react with hydroxyl radicals and thus act as inhibitors for the electrochemical oxidation reaction. These reactions may explain the presence of non-oxidized phenolic compounds at high Q values. However, further work is required to confirm this hypothesis.

4. Conclusions

Using porous solid DSA®-type of anodes having a Ti/$IrO_2/SnO_2/Sb_2O_5$ coating in a flow-through electrochemical system, it was demonstrated that a high TOC aqueous solution (5000 ppm) having a mixture of 3500 ppb of cresols and phenol was practically freed from these contaminants. After two pre-treatment steps for pH adjustment and filtration, only 20 ppb of *p*-cresol was present after 50 kC of charge was passed through the reactor treating 3 l of wastewater. The destruction of the phenolic compounds was achieved at the anode by indirect electrochemical oxidation through the production of highly reactive OH radicals and, thus, a low applied current density was necessary to avoid the competitive oxygen evolution reaction. Flow rate and the number of electrodes used were also factors to be considered: at low flow rates, reaction efficiency was improved due to greater residence times for the organic molecules inside the reactor. However, it has been demonstrated that it was crucial to set up the electrolysis reactor according to the optimum current density before increasing the total anode surface area and fixing the operating flow rate. Finally, this work confirmed the hypotheses of other authors indicating that the *p*-cresol was more rapidly oxidized into other species compared to the phenol, *o*- and *m*-cresol species.

Acknowledgements

The authors wish to thank Marie-Josée Lessard and Michel Thibodeau for their precious technical work regarding electrode preparation, electrolysis experiments as well as SEM studies.

References

1. Quebec Gouvernement Regulation,«Critères de qualité de l'eau de surface au Québec», Environnement Québec, (SERT, 1990 and MDEQ, 1997).
2. Quebec Gouvernement Regulation,«Règlement sur les fabriques de pâtes et papiers», Environnement Québec, (Q-2, r12.1, 1992).
3. M.D. Aitken, I.J. Massey, T. Chen and P.E. Heck, *Wat. Res.* **28** (1994) 1879.
4. A. Mylonas, E. Papaconstantinou and V. Roussis, *Polyhedron* **15** (1996) 3211.
5. S. Preis, Y. Terentyeva and A. Rozkov, *Wat. Sci. Tech.* **35** (1997) 165.
6. D.R. Lovley and D.J. Lonergan, *Appl. Environ. Microbiol.* **56** (1990) 1858.
7. Y. Zheng, D.O. Hill and C.H. Kuo, *J. Hazardous Mater.* **34** (1993) 245.
8. R. Kunin, *Poly. Eng. Sci.* **17** (1977) 58.
9. H. Sharifian and D.W. Kirk, *J. Electrochem. Soc.* **133** (1986) 921.
10. O.J. Murphy, G.D. Hitchens, L. Kaba and C.E. Verostko, *Wat. Res.* **26** (1992) 443.
11. C. Seignez, C. Pulgarin, P. Péringer, C. Comninellis and E. Plattner, *Swiss Chem.* **14** (1992) 25.
12. C. Comninellis, *Informations Chimie* **357** (1994) 109.
13. K.M. Petrov, L.M. Kaba, S. Srinivasan and A.J. Appleby, *Int. J. Hyrdogen Energy* **18** (1993) 377.
14. Y.M. Henuset and J. Fournier, U.S. Patent Application (2002).
15. L. Lipp and D. Pletcher, *Electrochim. Acta* **42** (1997) 1091.
16. R. Kötz, S. Stucki and B. Carcer, *J. Appl. Electrochem.* **21** (1991) 14.
17. F. Walsh, in 'A First Course in Electrochemical Engineering', (Ed.), (The Electrochemical Consultancy, Romsey, England, 1993), p. 142.
18. C. Comninellis and A. Nerini, *J. Appl. Electrochem.* **29** (1995) 23.
19. see Ref. [17], p. 245.
20. C. Comninellis, *Electrochim. Acta* **39** (1994) 1857.
21. U. Leffrang, K. Ebert, K. Flory, U. Gala and H. Schmieder, *Sep. Sci. Technol.* **30** (1995) 1883.
22. Y. Song and P.N. Pintauro, *J. Appl. Electrochem.* **21** (1991) 21.
23. R. Menini, A. Martel, H. Ménard, J. Lessard and O. Vittori, *Electrochim. Acta* **43** (1998) 1697.
24. C. Comninellis and C. Pulgarin, *J. Appl. Electrochem.* **21** (1991) 703.
25. W.H. Glaze and J.W. Kang, *Ind. Eng. Chem. Res.* **28** (1989) 1580.